UC Merced

Proceedings of the Annual Meeting of the Cognitive Science Society

Title

A Deep Entanglement Model of Attentional Bottleneck: Brain Plays Psi-Phi Plus Dice

Permalink

https://escholarship.org/uc/item/7486q3x5

Journal

Proceedings of the Annual Meeting of the Cognitive Science Society, 48(0)

Author

Sohrabi, Ahmad

Publication Date

2026

Copyright Information

This work is made available under the terms of a Creative Commons Attribution License, available at https://creativecommons.org/licenses/by/4.0/

Peer reviewed

eScholarship.org Powered by the California Digital Library University of California

A Deep Entanglement Model of Attentional Bottleneck: Brain Plays Psi-Phi Plus Dice

Ahmad Sohrabi[1] (ahmadsohrabi@cunet.carleton.ca)
[1]Department of Cognitive Science, Carleton University

Abstract

Human attention exhibits an attentional bottleneck during which conscious perception is impaired, a phenomenon that has not yet been explored directly with quantum models. This emerges when competing stimuli are presented serially and briefly. The representation of the stimuli was encoded as two-qubit entangled states, either correlated or anticorrelated. The mask intensity was encoded through random angle rotations to a qubit. The two qubits formed Bell states (Psi and Phi), undergoing deep entanglement through repeated layers. Measurement in terms of probability at each depth level simulated the attentional refraction and oscillation consistent with patterns observed in human studies, supported by extra measurements altogether, such as separate and combined probabilities, expectation values, and measures including entropy, fidelity, and concurrence. The model reproduced several effects found in attentional blink, specifically the well-known lag-1 sparing and masking effects, as well as two additional effects newly termed as partial lag-2 sparing and lag-7 divergence.

Keywords: Attentional Bottleneck; Quantum Depth; Masking; Cognitive Models

Introduction

Like many other cognitive processes, human attention exhibits fluctuations when processing rapidly presented stimuli, causing a bottleneck refractory period during which making decisions on the stimuli visibility or meaning is significantly affected. This refractory dynamical effect is the underlying mechanism involved in several phenomena such as Attentional Blink (AB), Masked Priming (MP), and many similar paradigms generally known as Rapid Serial Visual Presentation (RSVP; e.g., Potter, 1984), i.e., the double-slit-like experiments of cognitive science.

Using common AB paradigms, studies have shown that the visibility of a target stimulus (T2) presented shortly after a previous one (T1) can be successfully reported when their Stimulus Onset Asynchrony (SOA) is short enough, known as lag-1 sparing. Otherwise, the T2 is often rendered invisible during the refractory period of attention (e.g., Raymond et al., 1992; Chun & Potter, 1995; Nieuwenhuis et al., 2005), spanning lags 2 to 7 or even longer. The lag-1 sparing can be found if T2 is presented immediately around 100 msec from the T1 (e.g., Gao et al., 2020). The whole period of AB regularly has a U-shaped pattern, with a decrease to its trough followed by a recovery (Raymond et al., 1992). However, the results differ across studies, and a typical U-Shaped pattern is not warranted. For example, some studies have found a sharp U-shaped almost like a V, reaching a trough early at lag 2. One such result has been found by Tang et al. (2022) where the AB emerges abruptly at lag 2 and recovers linearly and quickly by lag 5. Some other interesting effect can happen, for example a slow decline from lag 2 to lag 3, followed by an increase beginning at lag 4 onward, a narrow U-shaped with a lower lag 2, and a final steadiness or reduction around lag 7 (Chun & Potter, 1995; see also, Nieuwenhuis et al., 2005). This dynamic nature of AB takes around one second where T2 may become unconscious commonly starting at lag 2 around 200 msec from T1 onset and slowly recovers after lag 5, typically after half a second, though the maximum refraction may end up at later lags depending on the experimental conditions.

Recent studies continue to point out the detailed and challenging nature of AB paradigms. For example, the abovementioned study (Tang et al., 2022), used Gabor gratings stimuli widely used in psychophysics and consciousness where participants are required to determine the orientation. They found that AB decreases when the two target stimuli (T1 and T2) are similar, and at maximum when they are dissimilar enough in their representation. In another study (Tang et al., 2020), they also showed a correlation between human AB data and human Electroencephalography (EEG) measures concurrently, and a correlation of 'human accuracy' for similar and non-similar targets in mice with the visual cortex electrophysiological recordings (firing rate in passive perception) when measured in humans and mice separately. Also, they found a correlation between human accuracy and target similarity computed from deep neural network (AlexNet) representation (cosine similarity).

The classical neurocomputational models are widely used in cognitive science (e.g., Bowman et al., 2006; Sohrabi, 2025a). The dynamic types have already been used to simulate some human AB data but in most cases, they show domain specificity and a difficulty in aligning with human data well (Nieuwenhuis et al., 2005; for more details see Sohrabi, 2025b). The flexibility and nonlinearity of quantum models compared to Bayesian in general has also been

In G. Boleda, I. Dautriche, M. Maldonado, C. Saldana and T. Torrent (Eds.), *Proceedings of the 48th Annual Conference of the Cognitive Science Society* ©2026 the author(s). This work is licensed under a Creative Commons Attribution 4.0 International License (CC BY).

revealed recently (e.g., Huang et al., 2026). The neurodynamical models, like other classical models, even in their basic forms, require several parameters to be set. These models of AB (e.g., Nieuwenhuis et al., 2005; Amir et al., 2022) seem not flexible enough in diverse domains or for different experimental results, especially a partial lag 2 sparing, a monotonous recovery, and a decline around lag 7, all similarly true for masked priming (e.g., Bowman et al., 2006; Sohrabi & West, 2009; Sohrabi & West, n.d.).

Here, we employ a simple quantum model as a two-qubit entanglement system to simulate binary decision making in cognitive tasks consisting of a serial presentation of two target stimuli with or without masks (distractors). The stimuli visibility is encoded as quantum states, i.e., either correlated or anticorrelated state pairs, and the masks as random rotation of angles. We try to simulate AB through implementation of Bell states (based on Psi or Phi) processed by a novel "deep entanglement channel" through repeated layers of gates, previously explored and employed for similar purposes (Sohrabi, 2025a; 2025b) but not in a straightforward and comprehensive way as here. We call it deep entanglement similar to what has been referred to as complexity depth (Sohrabi, 2025a) and deep teleportation (Sohrab, 2025b).

Current Study

A widely used approach for quantum modelling of information processing involves encoding data into qubits, for the purpose of relevant transformations and simulations. The quantum states will be represented as state vectors in the form of complex numbers realized on ansatz circuits (for some details see also, Sohrabi 2025a; 2025b). Each circuit contains a series of gates configured for a specific purpose where superposition and entanglement play the main role, creating an entanglement depth. It is more specific than the common term quantum depth where the number of qubits determines the width, and the serial arrangement of gates determines its length, making the final depth of the circuit. This main feature is essential and makes the model integrated, acting through a dynamic deep entanglement tunnel close to what is known as attentional bottleneck in psychology (Broadbent, 1958). It is mainly inspired by cognitive and biological studies, therefore called a quantum Cognitive Biological Model (qCBM; see also Sohrabi, 2025b).

As mentioned earlier regarding human data, our main aim in the study was to employ the qCBM as a basic model that can properly simulate the experimental results. For this purpose, we applied manipulations on angle values in a single qubit unitary gate (U) representing masking levels, ranging from weak to strong. In the current study, we fixed the entanglement through a CNOT gate to make the model simple and precise enough to increase its explanatory aspects, not to make it flexible for wider ranges of Attentional Blink (AB) found in human studies (see also Sohrabi, 2025b). We hypothesized that only by making systematic changes to the masking parameters, the typical U-Shaped AB pattern (hereafter, 7-lag U-Shaped) and a sharp U-Shaped pattern (hereafter, 5-lag V-Shaped) can be simulated, aligned with human data in Chun & Potter (1995) and Tang et al. (2022), respectively.

Methods

Ansatz Preparation

The qCBM is implemented via ansatz circuits consisting of two qubits used to prepare a state vector in Hilbert space ($|\psi\rangle \in H_4$) for representing the stimuli in Attentional Blink (AB). As shown in Figure 1, each depth level begins with a Hadamard gate (H) for superposition of the first qubit (hence, Qubit A). Then a U gate with random angle parameters is added to the second qubit (hence, Qubit B), acting as a mask (i.e., distractor) in human experiments. The main operation is an entanglement of the qubits through a CNOT control gate, i.e., a CX with Qubit A as the control and B as the target, simulating the attentional resources. The masking level is simulated using a U gate with randomly sampled rotation parameters on Qubit B as U(theta, phi, lambda, i.e., θ, φ, λ). At each level of depth, starting from 1 to N, a set of gates is iteratively applied, separated by barriers for visualization purpose in the current ideal simulations; an approach also useful in real hardware implementation. The simulations are carried out using the open-source IBM Qiskit library (Abhari et al., 2024).

The generated states are Bell states, consisting of all four states, having correlated ($|00\rangle$ or $|11\rangle$) and anticorrelated ($|01\rangle$ or $|10\rangle$) patterns, each with either + or – relative phase, i.e., Phi+ ($|\Phi+\rangle$), Phi- ($|\Phi -\rangle$), Psi+ ($|\Psi+\rangle$), and Psi- ($|\Psi-\rangle$). As illustrated separately in Figure 1 and discussed in next section, the simulation runs are performed each time on one of four ansatz circuits, depicted in separate rows, to generate four types of states, i.e., a Phi+ using H and CNOT gates, a Phi- by adding a Z on A, a Psi+ by adding an X on B, and finally a Psi-, by adding a Z on A, both followed by an extra X. This final correction makes the states Phi compatible to perform combined instead of separate visualization and analyses. This correction is made because the results of Psi and Phi separately were found to be similar but not uniform due to the so-called leakage when masking is used, i.e., having Psi among Phi and vice versa. The three parameters of masking were weighted differently for each masking condition, as will be described in the next section.

In the current software implementation, the operations are simulated using ideal unitary gates without introducing model noise but not executed on a physical quantum device. The depth resembles the number of layers in variational quantum algorithms (e.g., Bravo-Prieto et al., 2020). In the analysis, we encoded them as depth levels to simulate the typical lag numbers of stimuli presentation in the sample human studies, up to 8 lags, to show a bigger picture of common human studies. Knowing that the different measures of depth are linear, here the Qiskit depth measure of level 1-8 are 2-16 (up to 18 when all states included).

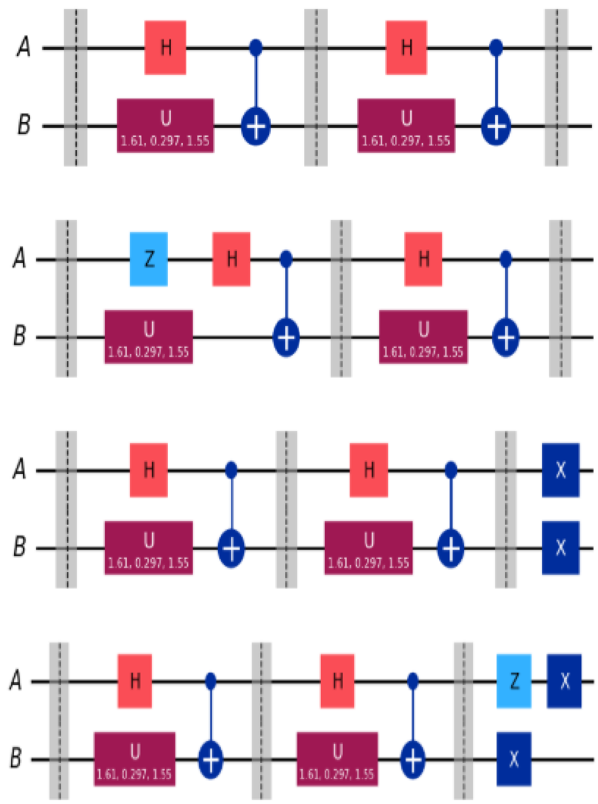

Figure 1. Examples of depth 2 in the qCBM model where unitary operations (H and U) are applied on single qubits, followed by an entanglement in the form of a CNOT gate with A as the control and B as the target. The circuits are customized to make all four entanglement types as shown in order from top to the bottom, The |Φ+⟩ using Hadamard and CNOT gates, then the |Φ-⟩ by adding a Z, the |Ψ+⟩ by adding an X, and finally the |Ψ-⟩ by adding a Z and an X, with an additional X applied for making Ψ states Φ-compatible.

Simulations

In each simulation, a state vector was generated from the parametrized ansatz to ultimately make a run for a total of 8 lags and 5 masking levels. The masking ranged randomly from 0 to a designated upper-bound, i.e., None (0π), Weak (4/10π), Thin (5/10 π), Thick (6/10π), and Strong (7/10π). A combination of the four Bell states and five masking levels created a given condition for each run (4096 runs for each cell), making up 20,480 for each depth level, ending up in 163,840 runs in total.

For simulation of the 5-lag V-Shaped pattern found in a mentioned study, all three parameters of masking (theta, phi, lambda, i.e., θ, φ, λ) had the same weights. However, for the slightly more complicated one, the 7-lag U-Shaped pattern, the theta, phi, and lambda were weighted at 1x, 2x, and 4x, respectively, with the same number of runs though repeating the None condition was redundant. All simulations could have been done by fewer runs (especially for None masking level) but as we had four Bell states and the common 1024 shots for each made the 4096 a reasonable number while extra runs did not make any noticeable differences (and less runs separates states in each correlated or anticorrelated pairs). The probability was calculated by squaring amplitudes |ψ| for analysis and visualization purposes.

We simply assume correlated (|00> and |11>) and anticorrelated (|01> and |10>) states represent visibility of both stimuli (T1 and T2) and only one of them, respectively (at representational not necessarily sensory level). Then the subtraction (correlated minus anticorrelated) will give a clearer picture, that can be assumed as reportability vs. blink. The mean value of the probability across runs for different conditions will be shown for correlated and anticorrelated as well as subtraction, to quantify the overall measurement. The subtraction value is closely related to the expectation value of a two-variable observable.

However, states correlation is not classical correlation, and assigning them to a specific cognitive representation is not easy but here rather arbitrary, e.g., they can be reversed by inverse or NOT gates, similar to what we did to make the states Phi compatible which causes alterations to the states. In addition to the probabilities as a measure of accuracy in human data, we also calculated entanglement degrees using entropy and concurrency to validate the results, as they are good indicators of the entanglement among qubits. Moreover, the fidelity among states of all depths was also calculated as an extra measure, reflecting similarity at different depths (lags). The measures reflect the effects of manipulating the angle values in the non-control unitary gate (U) as masking representation, and depth as lags in human data.

Results

For analyzing and visualizing the results, outcome probabilities were used as the main scale, along with entanglement measures including concurrence, entropy, and pairwise fidelity. The mean probability averaged across all relevant runs for correlated and anticorrelated states, as well as their subtraction, was calculated and illustrated using graphs for each masking condition. The mean probabilities of correlated and anticorrelated across all eight depths were opposite and almost symmetrical. Reportability accuracy can be treated either in terms of the probability of correlated states or similarly as the subtraction of correlated and anticorrelated state probabilities. As mentioned above, the latter is more relevant to the expectation value of a two-variable observable.

First, we examine the accuracy of both targets being seen, measured as the combined correlated states (|00> + |11>). As illustrated in Figure 2 (top-left), the graph shows the mean value of this measure for all masking levels (None or Weak to Strong). In the None condition, an asymmetric double staircase pattern was found, spanning all eight depths. Otherwise, the Weak to Strong masking conditions exhibited sharp U-Shaped (V-Shaped) patterns with a trough at lag 2 and a recovery around lag 4 or 6 for Strong and Weak masks, respectively. The overall pattern across all masking levels (except the None masking) is similar to the 5-lag V-Shaped patterns reported in the first study of interest (Tang et al., 2022). Stronger masking decreased the recovery at later lags, consistent with human data (Nieuwenhuis et al., 2005).

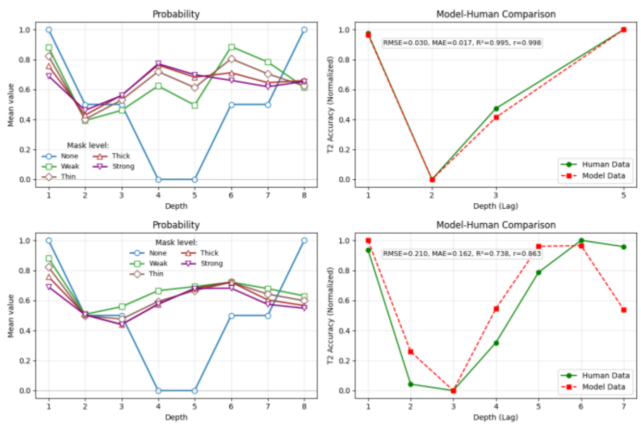

Figure 2. Mean probability as accuracy, defined as the combined probability for correlated states. Top-left shows a balanced double staircase pattern when no mask was used (None condition) spanning all eight depths; otherwise V-Shaped patterns are observed up to depth 4, followed by a decreasing oscillation under the Strong masking condition, for the first model-human comparison. Top-right shows the same data restricted to lags up to 5, demonstrating a good fit for this first model-human comparison, i.e., a 5-lag V-Shaped pattern. Bottom-left shows similar data but using non-uniform masking weights corresponding to the 7-lag U-Shaped patterns for the second model-human comparison. Bottom-right shows the same data restricted to lags up to 7, simulated by the model with acceptable agreement, as reflected in the reported fit measures, for this second model-human comparison, i.e., a 7-lag U-Shaped pattern.

Using the same data, Figure 2 (top-right) shows results restricted to lag 5 under the Strong masking condition, allowing a more direct model-human comparison. It excludes lag 4, since it was not measured in that study of interest (Tang et al., 2022). The 5-lag V-Shaped human data was successfully simulated by the model with a very good fit quantified using the root mean squared error (RMSE), mean absolute error (MAE), coefficient of determination (R^2), and Pearson correlation (r) as 0.030, 0.017, 0.995, and 0.998, respectively. We used only the mean values of the human data, rather than the raw data (which were difficult to reconcile), and therefore did not calculate inferential statistics such as p-values or confidence intervals.

To simulate the results of the 7-lag U-Shaped patterns in the second target study (Chun & Potter, 1995), we used the same highest masking intensity (Strong) but applied non-uniform masking weights, as described in the Methods section. Figure 2 (bottom-left) shows the results where the Weak to Strong masking conditions exhibited U-Shaped patterns with a trough at lag 3 for stronger masks and a slow recovery peaking around lag 6. The overall pattern in all masking levels (except the Weak and None conditions) is similar to the 7-lag U-Shaped patterns reported in the mentioned study. As shown in Figure 2 (bottom-right), for the model-human comparison, only seven depths were included in the fitting since the target human study used seven lags. Again, a good fit was obtained for this simulation, quantified using RMSE, MAE, R^2, and r with the values of 0.210, 0.162, 0.738, and 0.863, respectively.

The same results are depicted in other figures from different perspectives to provide a more comprehensive understanding of the model outputs (Figures 3 and 4). Again, these results are shown only for the Strong masking level, which was used in the model-human comparison for the target studies. In addition to the accuracy based on the combined probability for correlated states (|00> + |11>) and the subtraction, these figures also present the probabilities for anticorrelated states (|01> + |10>), the probabilities for four separate states (|00>, |01>, |10>, and |11>), the fidelity, as well as the entropy and concurrence measures.

In Figure 3 (top-left), we can see the probability values for separate states closely correspond to these of the combined correlated and anticorrelated states in Figure 3 (top-right), from which data were previously extracted for the first model-human comparison (5-lag V-Shaped human data in Figure 2, top-right). The graph also includes the subtraction (combined correlated minus combined anticorrelated states) which closely resembles the combined correlated states alone. Also, Figure 3 presents additional measures, including concurrence and entropy (bottom-left), as well as fidelity (bottom-right), which are broadly consistent with the probability results to some extent. Interestingly, these measures show similar patterns at corresponding depths, most notably the fidelity at the first depth compared with subsequent depths.

Likewise, Figure 4 shows the simulation results for 7-lag U-Shaped patterns across eight depths (lags), where top-left depicts the probabilities for the individual states. Additionally, the top-right displays the combined correlated and anticorrelated states, from which data were extracted for the second model-human comparison (i.e., 7-lag U-Shaped human data in Figure 2, bottom-right). It also includes the subtraction, which once again resembles the combined correlated-states probability. It also shows entropy and concurrence (bottom-left) as well as fidelity (bottom-right), consistent with the probability results. The fidelity at depth 1 relative to subsequent depths shows a typical U-Shaped pattern in which, following an initial drop, it rises smoothly to a maximum peak and then slightly decreases again at lag 7, namely lag-7 divergence.

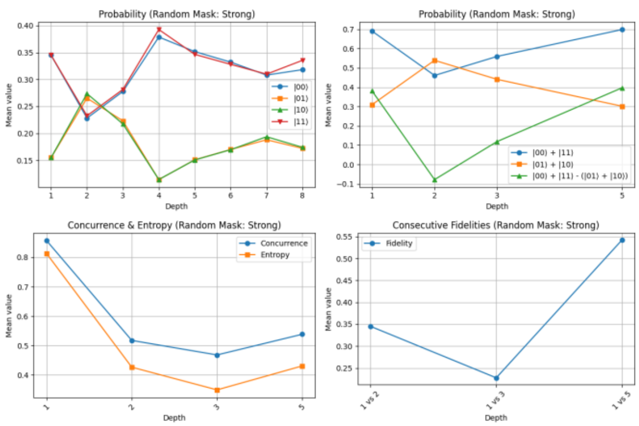

Figure 3. Simulation results for 5-lag V-Shaped patterns across all eight depths (lags) at the highest masking intensity (Strong). Top-left depicts the probabilities of the individual states, while top-right displays the combined correlated and anticorrelated states, from which data were extracted for model-human comparison. Top-right also shows the subtraction. Bottom-left shows entropy and concurrence, while bottom-right shows fidelity.

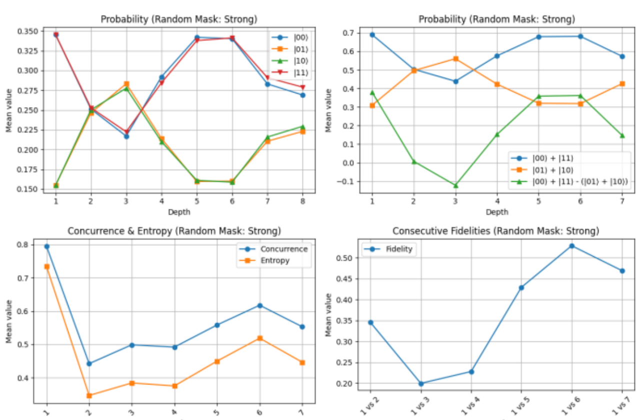

Figure 4. Simulation results for 7-lag U-Shaped patterns across all eight depths (lags) at the Strong level, using different masking weights. Top-left depicts the probabilities of the individual states, while top-right displays the combined correlated and anticorrelated states. Panel top-right also includes the subtraction. Bottom-left shows entropy and concurrence, while bottom-right shows fidelity as a typical U-Shaped pattern.

Finally, when no masks were used (None), the result was cleaner and more symmetrical but less similar to human data as shown in Figure 5. Interestingly, it still displays a U-Shaped pattern related to the attentional bottleneck that seems clearer and more intuitive, especially the subtraction measure when the whole eight depths are considered, in agreement with common U-Shaped AB duration. The same holds for fidelity, but concurrence and entropy showed abrupt changes, slightly more like the probability results for the five depths in the mentioned human data (V-Shaped).

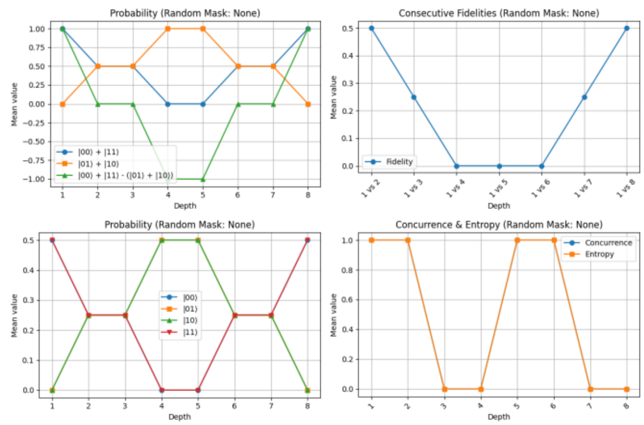

Figure 5. Simulation results for None masking condition. Top-left shows a U-Shaped pattern, especially evident in the subtraction measure, when all eight depths are considered. The same pattern holds for fidelity (top-right), but less evident for the individual states (bottom-left, with state pairs overlaid) and for concurrence and entropy (bottom-right), showing slightly better agreement with the probability results of the 5-lag V-Shaped human data.

Discussion

The quantum model we employed, based on a deep entanglement channel, successfully simulated a refractory period observed in attentional blink (AB). The representation of competing target stimuli was encoded through Bell state entanglement, in which phi and psi states undergo a deep quantum tunnel, analogous to an attentional bottleneck, long known in cognitive psychology (Broadbent, 1958; Deutsch & Deutsch, 1963; Treisman, 1964). This was achieved by encoding the visibility (reportability) of two targets while "measured" as probability outcomes of the correlated and anticorrelated states, corresponding to both targets being seen and only one target being seen, respectively. We used deep entanglement based simply on CNOT operations (i.e., psi and phi types) and random rotations on a single gate as masking noise, acting like a quantum dice.

The results showed the simulations of the well-known AB effects, a typical U-Shaped pattern found in previous studies (e.g., Chun & Potter, 1995) and a sharp U-Shaped (V-Shaped) pattern in other studies (e.g., Tang et al., 2022), only with a clean systematic masking parametrization. In addition to illustrating the well-known effects like lag 1 sparing and overall U-Shaped refractory period (e.g., Raymond et al., 1992; Chun & Potter, 1995), the model could show either a smooth or a steep drop to a trough (from lag 2 or onward) and a decrease after lag 5 to 7, especially with strong masks also found in human studies (Nieuwenhuis et al., 2005). The main outcome measure was the combined probability of the correlated states, but all other measures agreed with the patterns to some degrees, including entropy, fidelity, and concurrence. This also holds for the subtraction of combined correlated and anticorrelated states, which serves as another clear indicator of the typical U-Shaped period spanning approximately eight lags (Raymond et al., 1992).

The model captured the dynamic fluctuation of attention, especially AB (mainly related to neural refraction), through initial Bell psi phi states when simply undergoing a deep EPR-like channel. Unlike the deep teleportation method (Sohrabi, 2025b), we used probability measurements without classical bits-based Pauli corrections or extra qubits, to focus on the basic mechanism of attentional refractory period. We are not pointing to the exact neural realization of this cognitive process since it is hard to assume a detached underlying quantum state due to the embodied nature of cognition in the universe. However, this deep entanglement bottleneck may be seen at least partially as an implementation of microtubule tubulins, the proposed basis of Orch OR theory of consciousness (e.g., Hameroff & Penrose, 2014), something that requires further investigations.

The flexibility and nonlinearity of quantum models have been pointed out compared to classical neurocomputational (Sohrabi, 2025b) and Bayesian models (Huang et al., 2026). In the current model, we only manipulated the masking parameters in a clean systematic way. There is also still room for further parametrization, especially since we have new unpublished results using parametrized control gates that simulate human data from broader previous studies. However, here we tried to use parametrization in a constructive way (e.g., Mayer et al., 2010), rather than to arbitrarily fit data, referred to as “fit an elephant with four parameters” and with five, making “him wiggle his trunk”, a remark attributed to von Neumann (Dyson, 2004).

Although some effort have been made to model cognitive processes using quantum methods but so far most studies have been on less structured tasks like bistable perception (Atmanspacher & Filk, 2010) and have been highly mathematical (e.g., Buseymer et al., 2017), abstract (e.g., Buseymeyer & Lu, 2025), socio-emotional (e.g., Huang et al., 2025; 2026), or even hardware oriented (e.g., Pothukuchi et al., 2023). The current quantum inspired model is an attempt to start employing these models in a more cognitive modelling manner to systematically simulate basic cognitive processes backed by well-known experimental paradigms involving objective measures like Reaction Times (RT) and error, implemented in an explicit, well defined, and illustrative way (see also, Sohrabi, 2025b). These will pave ways for further involvement of cognitive scientists who are not engaged in common quantum cognition modeling.

Moreover, the state differences in the current model (i.e., correlated minus anticorrelated) can be imagined as the difference between congruent and incongruent prime-target relationship, known as Positive Congruency Effect (PCE) and Negative Congruency Effect (NCE), as lag 1 sparing and blink duration in Attentional Blink (AB), respectively. These effects are also related to target similarity (e.g., Tang et al., 2022), mask-target similarity (Raymond et al., 1995), and gradual target similarity effects (Karabay et al., 2022). Additionally, a sharp rise in RT early after shortest Stimulus Onset Asynchrony (SOA) (e.g., Schleghecken & Eimer, 2000; Sohrabi & West, 2008) and a gradual overall drop in RT at later lags (Jaśkowski & Ślósarek, 2007), have also been found in AB, related to accuracy in masking effects (Nieuwenhuis et al., 2005).

Therefore, the attentional bottleneck is not limited to Attentional Blink (AB) but reflects other relevant effects that all reveal cognitive representation strength as a continuum that gradually ends up producing strong effects, such as the binary-like phenomena in AB (Karabay et al., 2022). This is closely related to the entanglement in quantum that takes a form ranging from minimal to maximal along the initial superposition, similar to a notion known as representation strength (Sohrabi, 2008), showed up in relevant measures in the current study such as entropy, fidelity, and concurrence. This correlated and anticorrelated mirroring effect also can be seen as a cognitive resemblance of the symmetry effect in mathematics and physics as in Einstein-Rosen bridge (e.g., Gaztañaga et al., 2025), related to neuronal lateral inhibition, creating some dialectical phenomena as thesis and antithesis interaction (Sohrabi, 2008).

We do not assert that parsimony of models and theories is essential or universally applicable to global models, but to see the current basic model as a steppingstone for new approaches. As Feynman consistently puts forward, complex and novel phenomena arise from the repeated application of basic rules where meaning emerges from their relations and configurations (e.g., Feynman, 1965). This idea is close to what Gigerenzer (1991) and other cognitive scientists point out regarding the importance of rules including the fundamental if-then logic in reasoning (e.g., Anderson, 1990). However, mere rule-based models may not be flexible enough as we have seen with traditional (symbolic) AI and modeling approaches. They may work for higher level processes and social cognition, but even with their sub-symbolic improvements in ACT-R (e.g., Anderson & Lebiere, 1998), they may not adequately address micro-level mechanisms such as the attentional bottleneck.

Acknowledgements

The author thanks Robert West for his great comments.

References

Amir, N., Tishby, N., & Nelken, I. (2022). A simple model of the attentional blink and its modulation by mental training. *PLOS Computational Biology, 18*(8), e1010398. https://doi.org/10.1371/journal.pcbi.1010398

Anderson, J. R. (1990). An integrated theory of cognition. *American Psychologist, 45*(7), 724–739. https://doi.org/10.1037/0003-066X.45.7.724

Anderson, J. R., & Lebiere, C. (1998). *The atomic components of thought*. Lawrence Erlbaum Associates.

Atmanspacher, H., & Filk, T. (2010). A proposed test of temporal nonlocality in bistable perception. *Journal of Mathematical Psychology, 54*(3), *314–321.* https://doi.org/10.1016/j.jmp.2009.12.002

Bowman, H., Schlaghecken, F., & Eimer, M. (2006). A neural network model of inhibitory processes in subliminal priming. *Visual Cognition, 13*(4), 401–480.

Bravo-Prieto, C., Lumbreras-Zarapico, J., Tagliacozzo, L., & Latorre, J. I. (2020). Scaling of variational quantum circuit depth for condensed matter systems. *Quantum, 4*, 272. https://doi.org/10.22331/q-2020-05-28-272

Broadbent, D. E. (1958). *Perception and communication*. Pergamon Press.

Busemeyer, J. R., Fakhari, P., & Kvam, P. (2017). Neural implementation of operations used in quantum cognition. *Progress in Biophysics and Molecular Biology, 130*(Pt A), 53–60.

Busemeyer, J. & Lu, M. (2025). Quantum consciousness, brains, and cognition. Journal of Consciousness Studies, 32(9–10), 156–182.

Chun, M. M., & Potter, M. C. (1995). A two-stage model for multiple target detection in rapid serial visual presentation. *Journal of Experimental Psychology: Human Perception and Performance, 21*(1), 109–127.

Deutsch, J. A. & Deutsch, D. (1963). Attention: Some theoretical considerations, *Psychol. Rev.* 70, 80–90

Dyson, F. (2004). A meeting with Enrico Fermi. *Nature,* 427, 297.

Feynman, R. P. (1965). *The character of physical law*. MIT Press.

Gao, R., van den Brink, R. L., Pfeffer, T., & Voytek, B. (2020). Dynamic topographies of intrinsic neural timescales: A key role for consciousness. *Journal of Mathematical Psychology, 95*, 102327.

Gaztañaga, E., Kumar, K. S., & Marto, J. (2026). A new understanding of Einstein–Rosen bridges. *Classical and Quantum Gravity, 43*, 015023.

Gigerenzer, G. (1991). From tools to theories: A heuristic of discovery in cognitive psychology. *Psychological Review, 98*(2), 254–267.

Hameroff, S., & Penrose, R. (2014). Consciousness in the universe: A review of the "Orch OR" theory. *Physics of Life Reviews, 11*, 39–78.

Huang, J., Cohen, J., & Busemeyer, J. R. (2025). A quantum model of arousal and the Yerkes–Dodson law. In *Proceedings of the 47th Annual Meeting of the Cognitive Science Society*. Cognitive Science Society.

Huang, J., Zhang, Q., Xie, X., Breithaupt, F., & Busemeyer, J. R. (2026). A quantum model for serial reproduction. *Cognition, 266*, 106266.

Jaśkowski, P., & Ślósarek, M. (2007). How important is a prime's gestalt for subliminal priming? *Consciousness and Cognition, 16*(2), 485–497.

Javadi-Abhari, A., Treinish, M., Krsulich, K., Wood, C. J., Lishman, J., Gacon, J., & others. (2024). *Quantum computing with Qiskit* (arXiv Preprint No. arXiv:2405.08810). https://arxiv.org/abs/2405.08810

Karabay, A., Wilhelm, S. A., de Jong, J., Wang, J., Martens, S., & Akyürek, E. G. (2022). Two faces of perceptual awareness during the attentional blink: Gradual and discrete. *Journal of Experimental Psychology: General, 151*(7), 1520–1541. https://doi.org/10.1037/xge0001150

Mayer, J., Khairy, K., & Howard, J. (2010). Drawing an elephant with four complex parameters. American Journal of Physics, 78(6), 648–649.

Nieuwenhuis, S., Gilzenrat, M. S., Holmes, B. D., & Cohen, J. D. (2005). The role of the locus coeruleus in the regulation of cognitive performance. *Journal of Experimental Psychology: General, 134*(3), 291–307. https://doi.org/10.1037/0096-3445.134.3.291

Potter, M. C. (1984). Rapid serial visual presentation (RSVP): A method for studying language processing. In D. E. Kieras & M. A. Just (Eds.), *New methods in reading comprehension research* (pp. 91–118). Routledge.

Pothukuchi, R. P., Lufkin, L., Shen, Y. J., Simon, A., Thorstenson, R., Trevisan, B. E., Tu, M., & others. (2023). *The QUATRO application suite: Quantum computing for models of human cognition* (arXiv Preprint No. arXiv:2309.00597v2).

Raymond, J. E., Shapiro, K. L., & Arnell, K. M. (1992). Temporary suppression of visual processing in an RSVP task: An attentional blink? *Journal of Experimental Psychology: Human Perception and Performance, 18*(3), 849–860. https://doi.org/10.1037/0096-1523.18.3.849

Raymond, J. E., Shapiro, K. L., & Arnell, K. M. (1995). Similarity determines the attentional blink. *Journal of Experimental Psychology: Human Perception and Performance, 21*(3), 653–662.

Schlaghecken, F., & Eimer, M. (2000). A central–peripheral asymmetry in masked priming. *Perception & Psychophysics, 62*, 1367–1382.

Sohrabi, A. (2008). *Positive and negative congruency effects in masked and unmasked priming: Match of representation strength, attention and consciousness* (Doctoral dissertation). Carleton University Research Repository.

Sohrabi, A., & West, R. L. (2008). Positive and negative congruency effects in masked priming: A neuro-computational model based on representation strength and attention.*Nature Precedings*. npre.2008.2415.1

Sohrabi, A. (2025a). *Quantum depth for evaluating transformer-like models* (Technical Report No. 2025-02). Carleton University, Cognitive Science.

Sohrabi, A. (2025b). Deep teleportation: Quantum simulation of conscious report in attentional blink. *arXiv*. https://arxiv.org/pdf/2512.18585

Sohrabi, A., & West, R. L. (2009). Positive and negative congruency effects in masked priming: A neuro-computational model based on representation, attention, and conflict. *Brain Research, 1289*, 124–132.

Sohrabi, A., & West, R. L. (n.d.). The fragility of the reverse facilitation effect in the Stroop task: A dynamic neurocognitive model. *SSRN*. Doi:10.2139/ssrn.6683444

Tang, M., Shapiro, K. L., Enns, J. T., Visser, T. A. W., Mattingley, J. B., & Arabzadeh, E. (2022). Visual conscious awareness depends on a temporary filter based on representational similarity. *Research Square* (Preprint). https://doi.org/10.21203/rs.3.rs-2318730/v1

Tang, M. F., Ford, L., Arabzadeh, E., Enns, J. T., Visser, T. A. W., & Mattingley, J. B. (2020). Neural dynamics of the attentional blink revealed by encoding orientation selectivity during rapid visual presentation. *Nature Communications, 11*, 434.

Treisman, A. M. (1964). Selective attention in man, *Br. Med. Bull.* 20, 12–16.